Solution Synthesis of N = 8 Armchair Graphene Nanoribbons with High Charge Carrier Mobility

Xuelin Yao,[a,b*] Heng Zhang,[a] Fanmiao Kong,[b] Masanari Okuno,[c] Peter N. Horton,[d] Simon J. Coles,[d] Lapo Bogani,[b] Mischa Bonn,[a] Hai I. Wang,[a*] Klaus Müllen,[a*] and Akimitsu Narita[a,e*]

[a] Max Planck Institute for Polymer Research, Ackermannweg 10, 55128 Mainz, Germany

[b] Department of Materials, University of Oxford, OX1 3PH, Oxford, UK

[c] Department of Basic Science, Graduate School of Arts and Sciences, The University of Tokyo, 3-8-1 Komaba, Meguro, Tokyo 153-8902, Japan

[d] National Crystallography Service, School of Chemistry, University of Southampton, Southampton, SO17 1BJ, UK

[e] Organic and Carbon Nanomaterials Unit, Okinawa Institute of Science and Technology Graduate University, Okinawa 904-0495, Japan

ABSTRACT: Structurally defined graphene nanoribbons (GNRs) have emerged as promising candidates for nanoelectronic devices. Low bandgap (< 1 eV) GNRs are particularly important when considering the Schottky barrier in device performance. Here, we demonstrate the first solution synthesis of 8-AGNRs through a carefully designed arylated polynaphthalene precursor. The efficiency of the oxidative cyclodehydrogenation of the tailor-made polymer precursor into 8-AGNRs was validated by FT-IR, Raman, and UV-vis-near-infrared (NIR) absorption spectroscopy, and further supported by the synthesis of naphtho[1,2,3,4-*ghi*]perylene derivatives (**1** and **2**) as subunits of **8-AGNR**, with a width of 0.86 nm as suggested by the X-ray single crystal analysis. The resulting **8-AGNR** exhibited a remarkable NIR absorption extending up to ~2400 nm, corresponding to an optical bandgap as low as ~0.52 eV. Moreover, optical-pump TeraHertz-probe spectroscopy revealed a charge-carrier mobility in the dc limit of ~270 $cm^2 V^{-1} s^{-1}$ for the **8-AGNR**.

Graphene nanoribbons (GNRs) have appeared as promising candidates for next-generation nanoelectronics with their high charge-carrier mobilities and non-zero bandgaps.[1] Bottom-up synthesis, typically through on-surface or solution-mediated protocols, has provided atomically precise GNRs with diverse edge structures,[2-7] revealing not only their structure-dependent electronic and optical properties, but also the emergence of exotic topological phases[8, 9] and magnetic edge states.[10, 11] While GNRs with zigzag edges can be oxidized under air,[12] armchair GNRs (AGNR) are promising for electronic device applications considering their high stability and sizable bandgaps that are tunable by tailoring their width.[13-16]

AGNRs can be divided into three subfamilies of $N = 3p$, $N = 3p + 1$, and $N = 3p + 2$, where p is an integer and N denotes the rows of carbon atoms across the ribbon width.[13] In recent years, AGNRs of the first two subfamilies have been extensively investigated, confirming the predicted semiconducting properties with large bandgaps for $N = 7$, 9, and 13.[17-21] On the other hand, AGNRs that fall into the $N = 3p + 2$ subfamily are expected to possess excellent electrical properties, arising from their predicted low carrier effective masses, which lead to higher charge-carrier mobilities.[22-25] However, this subfamily of AGNRs has been relatively underexplored.

On-surface synthesis has successfully delivered 5-AGNRs,[26] the narrowest GNR of $N = 3p + 2$ subfamily, and a wider 17-AGNRs[27] with a small bandgap of 0.19 eV using tailor-made precursors. In addition, the lateral fusion of 3- and 5-AGNRs provided 8-AGNR fragments, and 14-AGNRs were concomitantly formed during the growth of 7-AGNRs,[28, 29] but their selective on-surface synthesis remains elusive.[30] Notably, Rubin et al. described the synthesis of 8-AGNRs through the solid-state Hopf pericyclic reaction of polydiacetylenes,[31] but the optical bandgap of the obtained sample was not reported presumably due to the insolubility. In comparison to the on-surface and solid-state synthesis methods that are constrained by limited processability of the resulting GNRs, solution-mediated synthesis can be an attractive alternative to enable the liquid-phase processing.[32, 33] A solution synthesis of 5-AGNRs was reported by alkyne benzannulation,[34] and also attempted by cyclodehydrogenation of poly(perylene),[35] but the wavelengths of their optical absorption edges were much shorter than expected from the theoretically predicted bandgap of 5-AGNRs.[13] Moreover, the solution synthesis of wider AGNRs belonging to the $N = 3p + 2$ subfamily has remained challenging

Herein we report the solution-synthesis of 8-AGNRs through the Scholl reaction of an arylated polynaphthalene precursor. The successful formation of 8-AGNRs was corroborated by Fourier-transform infrared (FT-IR) and Raman spectroscopy, as well as supported by the highly efficient synthesis of naphtho[1,2,3,4-*ghi*]perylene derivatives(**1** and **2**) as model compounds. Remarkably, the resulting 8-AGNRs revealed a near-infrared (NIR) absorption extending up to 2400 nm, corresponding to an optical bandgap of as low as 0.52 eV in line with the theoretical prediction.[36] Besides, time-resolved TeraHertz (THz) spectroscopy demonstrated a high

Scheme 1. Synthetic Routes to Compounds 1 and 2.

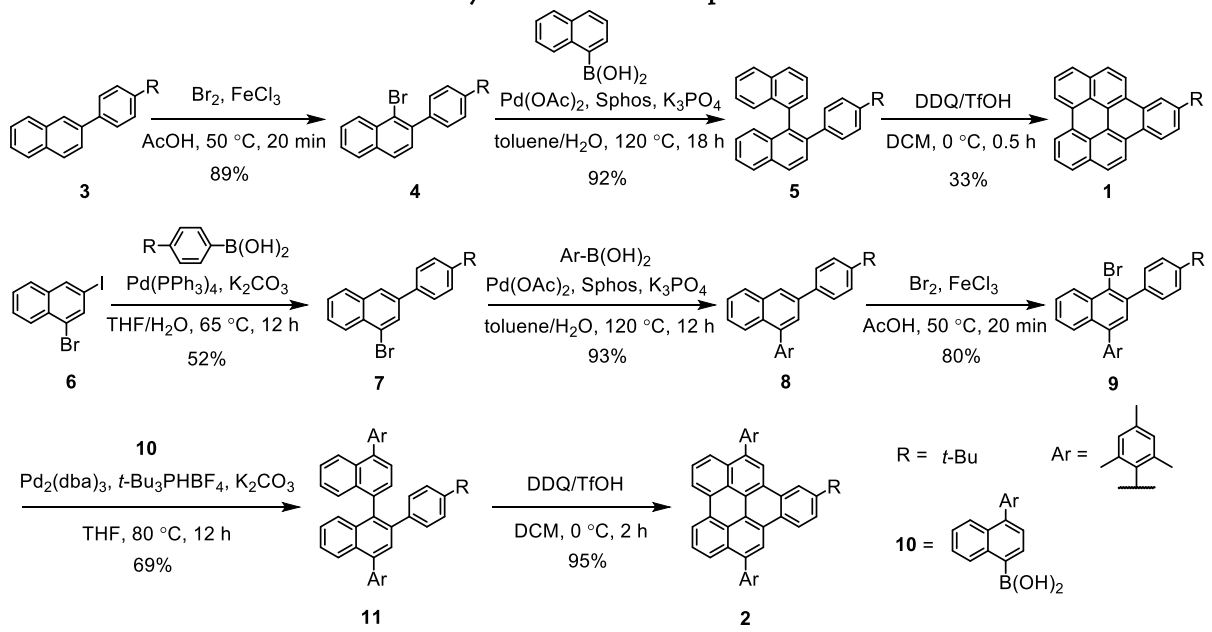

short-range charge-carrier mobility up to ~270 and ~170 $cm^2 V^{-1} s^{-1}$ in dispersion and the thin-film of **8-AGNR**, respectively, suggesting its great potential for applications in electronic devices.

The synthesis of naphtho[1,2,3,4-*ghi*]perylene derivatives (**1** and **2**) as model compound is depicted in Scheme 1. 2-[4-(*tert*-Butyl)phenyl]-1,1'-binaphthyl (**5**) was first synthesized through bromination of 2-[4-(*tert*-butyl)phenyl]naphthalene (**3**) to give 1-bromo-2-[4-(*tert*-butyl)phenyl]naphthalene (**4**), followed by a Suzuki coupling with 1-naphthylboronic acid. The Scholl reaction of **5** with 2,3-dichloro-5,6-dicyano-1,4-benzoquinone (DDQ) /trifluoromethanesulfonic acid (TfOH) at 0 °C afforded **1** as a yellow solid in 33% yield. The low yield of **1** could be ascribed to a competing dimerization of **1** during the Scholl reaction, as indicated by mass spectroscopy results (see Figure S1). A similar dimerization of triphenylene was reported under the Scholl reaction of unsubstituted *o*-terphenyl.[37] To circumvent this issue, we re-designed the model structure to compound **2**, introducing bulky substituents, i.e., mesityl groups, on the naphtho[1,2,3,4-*ghi*]perylene core. Toward the synthesis of 2-[4-(*tert*-butyl)phenyl]-4,4'-dimesityl-1,1'-binaphthalene (**11**) as the precursor of **2**, 1-bromo-3-iodonaphthalene (**6**) was initially prepared (see synthetic details in supporting information (SI)). Two aryl groups were then installed sequentially at the naphthalene core of **6** via selective Suzuki coupling, followed by bromination to give 1-bromo-2-[4-(*tert*-butyl)phenyl]-4-mesitylnaphthalene (**9**). Subsequently, Suzuki coupling of **9** with (4-mesitylnaphthalen-1-yl)boronic acid (**10**) provided **11** in 69% yield. Cyclodehydrogenation of **11** with DDQ/TfOH furnished compound **2** in an excellent yield of 95% and no dimerized product was detected by mass spectrometry (Figure S2).

Compounds **1** and **2** were initially characterized by matrix-assisted laser desorption/ionization time-of-flight mass spectrometry (MALDI–TOF MS), which displayed the expected molecular mass, and NMR spectroscopy showed well-resolved proton signals that could be fully assigned (see MALDI-TOF MS and NMR spectra in SI). Moreover, single crystals suitable for the X-ray diffraction analysis could be obtained by slow evaporation of their solutions in dichloromethane, unambiguously revealing their structures (Figure 1). Compound **1** has a planar geometry while the aromatic core of **2** is slightly bent due to the mesityl groups. Both **1** and **2** adopt lamellar packing motifs, although the latter has a larger packing distance. Additionally, a width of 0.86 nm can be estimated for 8-AGNRs from the structure of **1** (Figure 1a).

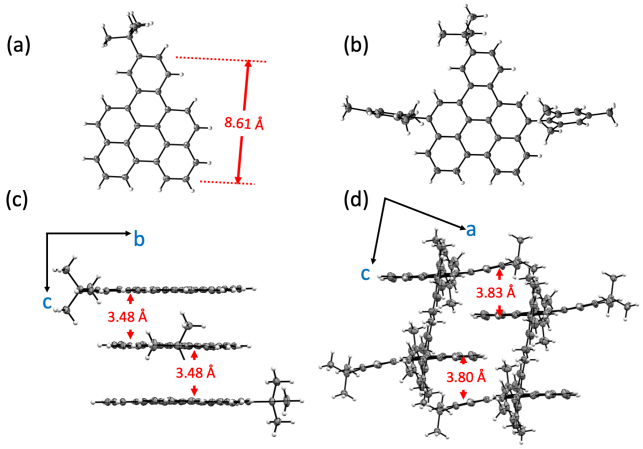

Figure 1. Crystal structures of compounds **1** and **2**. (a, b) ORTEP drawing of **1** and **2**, with thermal ellipsoids shown at 50% probability, respectively. (c, d) Crystal packings of **1** and **2**, respectively.

Encouraged by the successful synthesis of model compound **2**, the synthetic route to 8-AGNRs was designed as illustrated in Scheme 2. First, dibromoarene **13** was synthesized by silver-mediated direct arylation of 1,4-dibromonaphthalene with 1-(4-decylhexadecyl)-4-iodobenzene (**12**).[38] Subsequently, selective monolithiation/borylation of **13** furnished arylated naphthalene isomers **14** and **14'** functionalized with bromo and boronic ester groups, which could be easily separated by silica gel column chromatography (see SI for details). Palladium-catalyzed AB-type Suzuki polymerization of **14** provided arylated polynaphthalene precursor **P1** with pendent branched alkyl chains. After the removal of short oligomers via recycling gel permeation chromatography (GPC), analysis of **P1** by size exclusion chromatography (SEC) against linear polystyrene standard indicated a number-average molecular weight (M_n) of about 3.3×10^4 g mol^{-1} and a polydispersity index

Scheme 2. Schematic Illustration of the Synthesis of 8-AGNR.

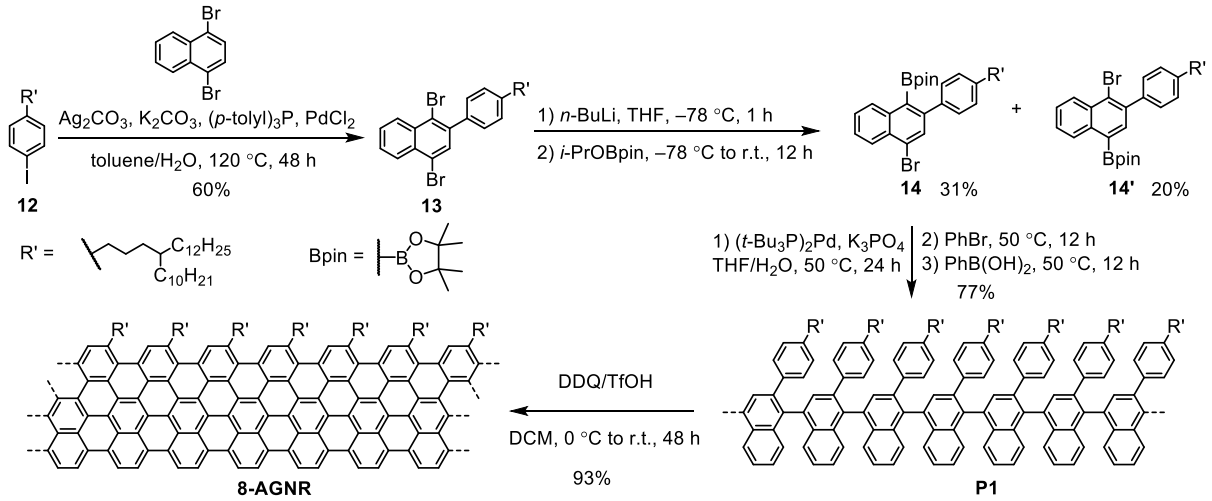

(PDI) of 2.0 (Figure S3). MALDI-TOF MS characterization revealed a regular pattern with peak-to-peak distance of ~567, corresponding to the molecular mass of the repeating unit (Figure S4). Finally, the Scholl reaction of **P1** with DDQ/TfOH in dichloromethane afforded **8-AGNR**. The estimated average length of **8-AGNR** is ~20 nm based on the SEC analysis of **P1**.

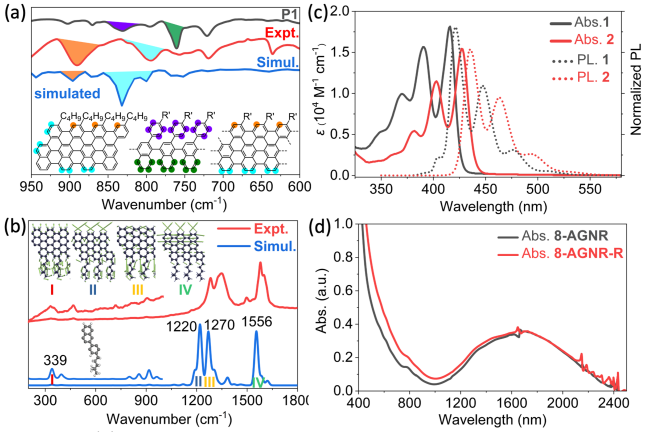

Figure 2. (a) FT-IR spectra of **P1** and **8-AGNR** measured on powder samples and DFT-simulated spectrum. (b) Raman spectrum of **8-AGNR** recorded with a 532 nm excitation laser on a powder sample. Inset: vibrational modes associated with simulated bands. (c) UV-vis and photoluminescence spectra of **1** and **2** (10^{-5} M) in THF. (d) UV-vis-NIR spectrum of **8-AGNR** and **8-AGNR-R** (after treatment with hydrazine) in 1,2,4-trichlorobenzene (0.1 mg/mL).

The successful transformation of **P1** into **8-AGNR** via the Scholl reaction was initially corroborated by FT-IR spectroscopic analyses combined with density functional theory (DFT) simulations (Figure 2a). Distinct C–H out-of-plane (*opla*) vibrational modes, defined as SOLO, DUO, and QUATRO which are strongly associated with the number of adjacent C–H bonds (highlighted with different colors in Figure 2a),[39] provide a precise fingerprinting of the molecular structures. **P1** is characterized by the QUATRO mode at 761 cm^{-1} (olive-colored), which is significantly attenuated in the spectrum of **8-AGNR**, indicating the efficient cyclization of the polynaphthalene backbone in **P1**. Compared with the spectrum of **P1**, the *opla* band centered at 831 cm^{-1} (purple-colored) is absent in that of **8-AGNR**, in line with the annulation of the pendent phenyl rings.[31, 40] Based on the DFT simulation, two bands observed at 891 cm^{-1} (orange-colored) and 801 cm^{-1} (cyan-colored) in the spectrum of **8-AGNR** are assignable to the SOLO and DUO modes, respectively, corroborating the armchair-edged structure of **8-AGNR**.

The experimental Raman spectrum of **8-AGNR** revealed a good agreement with the DFT-calculated one (Figure 2b), which further supports the successful formation of 8-AGNRs. In general, three peaks of **8-AGNR** centered at 1578, 1345, and 1281 cm^{-1} can be assigned to G, D, and edge C–H peaks, respectively, by comparing with the simulated spectrum. The G peak shows a splitting with a shoulder peak at 1598 cm^{-1}, which can be ascribed to the frequency splitting of the longitudinal and transverse optical modes in AGNRs.[41] An absorption peak at the low-energy spectral region is observed at 336 cm^{-1} for **8-AGNR**. This peak is assignable to the radial breathing-like mode (RBLM) according to DFT simulation. Following a zone-folding model,[42] the frequency of RBLM (ω_{RBLM}) is linked to the width of GNR (w_{GNR}) via $\omega_{RBLM} = 3222$ Å cm^{-1} / w_{GNR}. The width of **8-AGNR** is thus estimated to be 0.96 nm, which is fully consistent with crystallographic results of model compound **1**.

The UV-vis absorption spectra of **1** and **2** (Figure 2c) present the longest absorption band at 416 and 427 nm, respectively, along with the optical energy gap of 2.91 and 2.82 eV according to the absorption onset, displaying the lowering of the energy gap by the mesityl groups. The fluorescence spectra of **1** and **2** depict a symmetrical pattern with their absorption spectrum and a small Stokes shift of 5 (286 cm^{-1}) and 9 nm (484 cm^{-1}), respectively, indicating their rigid framework. Compared to **1** and **2**, the absorption of **8-AGNR** dispersed in 1,2,4-trichlorobenzene highlights an extensive red-shift into the NIR region with a broad absorption peak at 1700 nm (Figure 2d). To exclude the contribution of possible oxidized cationic species,[35, 43] like radical cations or dications that could be formed under the Scholl reaction, **8-AGNR** was further treated with hydrazine, furnishing a nearly identical spectrum (Figure 2d). Based on the absorption onset, we deduce a record narrow optical bandgap of 0.52 eV for **8-AGNR**, in line with the theoretically predicted optical bandgap of 0.42 eV.[36] This finding further corroborates the successful formation of 8-AGNRs.

Optical-pump THz-probe (OPTP) spectroscopy was applied to study the electrical properties of **8-AGNR**. Figure 3a displays the ultrafast complex photoconductivity dynamics of **8-AGNR** dispersed

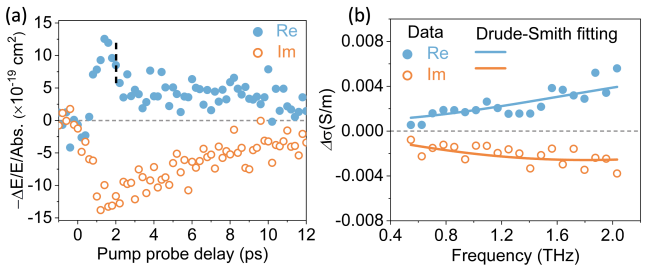

Figure 3. (a) THz photoconductivity dynamics of **8-AGNR** following photoexcitation, normalized to the absorbed photon density. (b) Frequency-resolved THz photoconductivity measured at 2 ps (marked by the dashed vertical line in (a)) after photoexcitation. The solid lines are fits to the Drude-Smith model.

in 1,2,4-trichlorobenzene. A rapid, picosecond rise of photoconductivity ($\Delta\sigma$) is assigned to free carrier generation in GNRs upon photoexcitation (by 3.10 eV laser pulses). Furthermore, the frequency-resolved THz conductivity recorded near the peak photoconductivity (Figure 3b) is well-described by the Drude-Smith (DS) mode (see SI). The DS mode describes the transport of free charges experiencing backscattering processes, arising from, e.g., grain boundaries and structural distortions.[4, 44] A parameter c, ranging from 0 (no backscattering, giving the Drude model response) to −1 (complete backscattering), characterizes the backscattering probability. From the fitting, a charge scattering time τ = 35 ± 6 fs and c = −0.93 ± 0.03 can be derived. A short-range charge mobility in the dc limit of ~270 ± 4 $cm^2\ V^{-1}\ s^{-1}$ can be inferred following: $\mu_{dc} = \frac{e\tau}{m^*}(1 + c)$, m^* = 0.0163 m_0 (see SI). This value represents a record-high value among the reported GNRs (vs ~20 − 30 $cm^2\ V^{-1}\ s^{-1}$ for the previous record in GNRs by the same technique[5]) which largely originates from the intrinsically small charge carrier effective masses in 8-AGNRs. Finally, the transport properties of **8-AGNR** in a thin film formed by drop-casting were tested (see SI). A larger τ = 46 ± 6 fs and c = −0.97 ± 0.03 are obtained. We thus infer a μ_{dc} of ~170 ± 2 $cm^2\ V^{-1}\ s^{-1}$ in the film geometry, highlighting the great potential of **8-AGNR** for applications in organic filed-effect transistors and photovoltaics, where high mobility is essential for efficient charge transport.

In summary, we demonstrate the first synthesis of 8-AGNRs in solution via an arylated polynaphthalene precursor. Remarkably, the prepared **8-AGNR** exhibit a significant NIR absorption up to 2400 nm and a narrow optical bandgap of 0.52 eV. A photoconductivity investigation of **8-AGNR** viaTHz spectroscopy indicated a high local charge-carrier mobility of ~270 and ~170 $cm^2\ V^{-1}\ s^{-1}$ in dispersion and thin-film of **8-AGNR**, respectively, highlighting this **8-AGNR** as a promising candidate for electronic devices. Furthermore, the novel polymer design strategy developed in this work can facilitate the synthesis of wider AGNRs falling within $N = 3p + 2$ subgroup, like 11-AGNRs, 14-AGNRs, 17-AGNRs, etc, by simply changing the aryl substituent. Therefore, our study will also open a door for the long-pursued metallic GNRs in solution and further explore their physiochemical properties.

ASSOCIATED CONTENT

Supporting Information

Supporting Information. The Supporting Information is available free of charge at http://pubs.acs.org."

Experimental details and theoretical calculations (PDF)
X-ray crystallographic data for **1** (CCDC 2243983) (CIF)
X-ray crystallographic data for **2** (CCDC 2243984) (CIF)

AUTHOR INFORMATION

Corresponding Author

*E-mail: xuelin.yao@materials.ox.ac.uk
*E-mail: wanghai@mpip-mainz.mpg.de
*E-mail: muellen@mpip-mainz.mpg.de
*E-mail: akimitsu.narita@oist.jp

Notes

The authors declare no competing financial interest.

ACKNOWLEDGMENT

This work was financially supported by the Max Planck Society, the FLAG-ERA Grant OPERA by DFG 437130745, and JSPS KAKENHI (Grant Number 21KK0091). X. Yao is grateful for Marie Skłodowska-Curie Research Fellowship (894761-MolecularMAGNET). The authors would like to acknowledge the use of the University of Oxford Advanced Research Computing (ARC) facility.

REFERENCES

(1) Wang, H.; Wang, H. S.; Ma, C.; Chen, L.; Jiang, C.; Chen, C.; Xie, X.; Li, A.-P.; Wang, X. Graphene nanoribbons for quantum electronics. *Nat. Rev. Phys.* **2021**, *3*, 791-802.
(2) Yao, X.; Zheng, W.; Osella, S.; Qiu, Z.; Fu, S.; Schollmeyer, D.; Müller, B.; Beljonne, D.; Bonn, M.; Wang, H. I.; Müllen, K.; Narita, A. Synthesis of Nonplanar Graphene Nanoribbon with Fjord Edges. *J. Am. Chem. Soc.* **2021**, *143*, 5654-5658.
(3) Niu, W.; Ma, J.; Soltani, P.; Zheng, W.; Liu, F.; Popov, A. A.; Weigand, J. J.; Komber, H.; Poliani, E.; Casiraghi, C.; Droste, J.; Hansen, M. R.; Osella, S.; Beljonne, D.; Bonn, M.; Wang, H. I.; Feng, X.; Liu, J.; Mai, Y. A Curved Graphene Nanoribbon with Multi-Edge Structure and High Intrinsic Charge Carrier Mobility. *J. Am. Chem. Soc.* **2020**, *142*, 18293-18298.
(4) Narita, A.; Feng, X.; Hernandez, Y.; Jensen, S. A.; Bonn, M.; Yang, H.; Verzhbitskiy, I. A.; Casiraghi, C.; Hansen, M. R.; Koch, A. H. R.; Fytas, G.; Ivasenko, O.; Li, B.; Mali, K. S.; Balandina, T.; Mahesh, S.; De Feyter, S.; Müllen, K. Synthesis of structurally well-defined and liquid-phase-processable graphene nanoribbons. *Nat. Chem.* **2014**, *6*, 126-132.
(5) Wang, X.; Ma, J.; Zheng, W.; Osella, S.; Arisnabarreta, N.; Droste, J.; Serra, G.; Ivasenko, O.; Lucotti, A.; Beljonne, D.; Bonn, M.; Liu, X.; Hansen, M. R.; Tommasini, M.; De Feyter, S.; Liu, J.; Wang, H. I.; Feng, X. Cove-Edged Graphene Nanoribbons with Incorporation of Periodic Zigzag-Edge Segments. *J. Am. Chem. Soc.* **2022**, *144*, 228-235.
(6) Cai, J.; Pignedoli, C. A.; Talirz, L.; Ruffieux, P.; Söde, H.; Liang, L.; Meunier, V.; Berger, R.; Li, R.; Feng, X.; Müllen, K.; Fasel, R. Graphene nanoribbon heterojunctions. *Nat. Nanotechnol.* **2014**, *9*, 896-900.
(7) de Oteyza, D. G.; García-Lekue, A.; Vilas-Varela, M.; Merino-Díez, N.; Carbonell-Sanromà, E.; Corso, M.; Vasseur, G.; Rogero, C.; Guitián, E.; Pascual, J. I.; Ortega, J. E.; Wakayama, Y.; Peña, D. Substrate-Independent Growth of Atomically Precise Chiral Graphene Nanoribbons. *ACS Nano* **2016**, *10*, 9000-9008.
(8) Rizzo, D. J.; Veber, G.; Cao, T.; Bronner, C.; Chen, T.; Zhao, F.; Rodriguez, H.; Louie, S. G.; Crommie, M. F.; Fischer, F. R. Topological band engineering of graphene nanoribbons. *Nature* **2018**, *560*, 204-208.
(9) Gröning, O.; Wang, S.; Yao, X.; Pignedoli, C. A.; Borin Barin, G.; Daniels, C.; Cupo, A.; Meunier, V.; Feng, X.; Narita, A.; Müllen, K.; Ruffieux,

P.; Fasel, R. Engineering of robust topological quantum phases in graphene nanoribbons. *Nature* **2018**, *560*, 209-213.
(10) Blackwell, R. E.; Zhao, F.; Brooks, E.; Zhu, J.; Piskun, I.; Wang, S.; Delgado, A.; Lee, Y.-L.; Louie, S. G.; Fischer, F. R. Spin splitting of dopant edge state in magnetic zigzag graphene nanoribbons. *Nature* **2021**, *600*, 647-652.
(11) Ruffieux, P.; Wang, S.; Yang, B.; Sánchez-Sánchez, C.; Liu, J.; Dienel, T.; Talirz, L.; Shinde, P.; Pignedoli, C. A.; Passerone, D.; Dumslaff, T.; Feng, X.; Müllen, K.; Fasel, R. On-surface synthesis of graphene nanoribbons with zigzag edge topology. *Nature* **2016**, *531*, 489-492.
(12) Liu, J.; Ravat, P.; Wagner, M.; Baumgarten, M.; Feng, X.; Müllen, K. Tetrabenzo[a,f,j,o]perylene: A Polycyclic Aromatic Hydrocarbon With An Open-Shell Singlet Biradical Ground State. *Angew. Chem. Int. Ed.* **2015**, *54*, 12442-12446.
(13) Son, Y.-W.; Cohen, M. L.; Louie, S. G. Energy Gaps in Graphene Nanoribbons. *Phys. Rev. Lett.* **2006**, *97*, 216803.
(14) Nakada, K.; Fujita, M.; Dresselhaus, G.; Dresselhaus, M. S. Edge state in graphene ribbons: Nanometer size effect and edge shape dependence. *Phys. Rev. B* **1996**, *54*, 17954-17961.
(15) Barone, V.; Hod, O.; Scuseria, G. E. Electronic Structure and Stability of Semiconducting Graphene Nanoribbons. *Nano Lett.* **2006**, *6*, 2748-2754.
(16) Yang, L.; Park, C.-H.; Son, Y.-W.; Cohen, M. L.; Louie, S. G. Quasiparticle Energies and Band Gaps in Graphene Nanoribbons. *Phys. Rev. Lett.* **2007**, *99*, 186801.
(17) Li, G.; Yoon, K.-Y.; Zhong, X.; Wang, J.; Zhang, R.; Guest, J. R.; Wen, J.; Zhu, X. Y.; Dong, G. A modular synthetic approach for band-gap engineering of armchair graphene nanoribbons. *Nat. Commun.* **2018**, *9*, 1687.
(18) Cai, J.; Ruffieux, P.; Jaafar, R.; Bieri, M.; Braun, T.; Blankenburg, S.; Muoth, M.; Seitsonen, A. P.; Saleh, M.; Feng, X.; Müllen, K.; Fasel, R. Atomically precise bottom-up fabrication of graphene nanoribbons. *Nature* **2010**, *466*, 470-473.
(19) Chen, Y.-C.; de Oteyza, D. G.; Pedramrazi, Z.; Chen, C.; Fischer, F. R.; Crommie, M. F. Tuning the Band Gap of Graphene Nanoribbons Synthesized from Molecular Precursors. *ACS Nano* **2013**, *7*, 6123-6128.
(20) Di Giovannantonio, M.; Deniz, O.; Urgel, J. I.; Widmer, R.; Dienel, T.; Stolz, S.; Sánchez-Sánchez, C.; Muntwiler, M.; Dumslaff, T.; Berger, R.; Narita, A.; Feng, X.; Müllen, K.; Ruffieux, P.; Fasel, R. On-Surface Growth Dynamics of Graphene Nanoribbons: The Role of Halogen Functionalization. *ACS Nano* **2018**, *12*, 74-81.
(21) Li, G.; Yoon, K.-Y.; Zhong, X.; Zhu, X.; Dong, G. Efficient Bottom-Up Preparation of Graphene Nanoribbons by Mild Suzuki–Miyaura Polymerization of Simple Triaryl Monomers. *Chem. Eur. J.* **2016**, *22*, 9116-9120.
(22) Bennett, P. B.; Pedramrazi, Z.; Madani, A.; Chen, Y.-C.; de Oteyza, D. G.; Chen, C.; Fischer, F. R.; Crommie, M. F.; Bokor, J. Bottom-up graphene nanoribbon field-effect transistors. *Appl. Phys. Lett.* **2013**, *103*, 253114.
(23) Llinas, J. P.; Fairbrother, A.; Borin Barin, G.; Shi, W.; Lee, K.; Wu, S.; Yong Choi, B.; Braganza, R.; Lear, J.; Kau, N.; Choi, W.; Chen, C.; Pedramrazi, Z.; Dumslaff, T.; Narita, A.; Feng, X.; Müllen, K.; Fischer, F.; Zettl, A.; Ruffieux, P.; Yablonovitch, E.; Crommie, M.; Fasel, R.; Bokor, J. Short-channel field-effect transistors with 9-atom and 13-atom wide graphene nanoribbons. *Nat. Commun.* **2017**, *8*, 633.
(24) Javey, A.; Guo, J.; Wang, Q.; Lundstrom, M.; Dai, H. Ballistic carbon nanotube field-effect transistors. *Nature* **2003**, *424*, 654-657.
(25) Dürkop, T.; Getty, S. A.; Cobas, E.; Fuhrer, M. S. Extraordinary Mobility in Semiconducting Carbon Nanotubes. *Nano Lett.* **2004**, *4*, 35-39.
(26) Kimouche, A.; Ervasti, M. M.; Drost, R.; Halonen, S.; Harju, A.; Joensuu, P. M.; Sainio, J.; Liljeroth, P. Ultra-narrow metallic armchair graphene nanoribbons. *Nat. Commun.* **2015**, *6*, 10177.
(27) Yamaguchi, J.; Hayashi, H.; Jippo, H.; Shiotari, A.; Ohtomo, M.; Sakakura, M.; Hieda, N.; Aratani, N.; Ohfuchi, M.; Sugimoto, Y.; Yamada, H.; Sato, S. Small bandgap in atomically precise 17-atom-wide armchair-edged graphene nanoribbons. *Commun. Mater.* **2020**, *1*, 36.
(28) Sun, K.; Ji, P.; Zhang, J.; Wang, J.; Li, X.; Xu, X.; Zhang, H.; Chi, L. On-Surface Synthesis of 8- and 10-Armchair Graphene Nanoribbons. *Small* **2019**, *15*, 1804526.
(29) Huang, H.; Wei, D.; Sun, J.; Wong, S. L.; Feng, Y. P.; Neto, A. H. C.; Wee, A. T. S. Spatially Resolved Electronic Structures of Atomically Precise Armchair Graphene Nanoribbons. *Sci. Rep.* **2012**, *2*, 983.
(30) Xu, X.; Kinikar, A.; Di Giovannantonio, M.; Ruffieux, P.; Müllen, K.; Fasel, R.; Narita, A. On-Surface Synthesis of Dibenzohexacenohexacene and Dibenzopentaphenoheptaphene. *Bull. Chem. Soc. Jpn.* **2021**, *94*, 997-999.
(31) Jordan, R. S.; Li, Y. L.; Lin, C.-W.; McCurdy, R. D.; Lin, J. B.; Brosmer, J. L.; Marsh, K. L.; Khan, S. I.; Houk, K. N.; Kaner, R. B.; Rubin, Y. Synthesis of N = 8 Armchair Graphene Nanoribbons from Four Distinct Polydiacetylenes. *J. Am. Chem. Soc.* **2017**, *139*, 15878-15890.
(32) Narita, A.; Chen, Z.; Chen, Q.; Müllen, K. Solution and on-surface synthesis of structurally defined graphene nanoribbons as a new family of semiconductors. *Chem. Sci.* **2019**, *10*, 964-975.
(33) Niu, W.; Sopp, S.; Lodi, A.; Gee, A.; Kong, F.; Pei, T.; Gehring, P.; Nägele, J.; Lau, C. S.; Ma, J.; Liu, J.; Narita, A.; Mol, J.; Burghard, M.; Müllen, K.; Mai, Y.; Feng, X.; Bogani, L. Exceptionally clean single-electron transistors from solutions of molecular graphene nanoribbons. *Nat. Mater.* **2023**, *22*, 180-185.
(34) Yang, W.; Lucotti, A.; Tommasini, M.; Chalifoux, W. A. Bottom-Up Synthesis of Soluble and Narrow Graphene Nanoribbons Using Alkyne Benzannulations. *J. Am. Chem. Soc.* **2016**, *138*, 9137-9144.
(35) Jänsch, D.; Ivanov, I.; Zagranyarski, Y.; Duznovic, I.; Baumgarten, M.; Turchinovich, D.; Li, C.; Bonn, M.; Müllen, K. Ultra-Narrow Low-Bandgap Graphene Nanoribbons from Bromoperylenes—Synthesis and Terahertz-Spectroscopy. *Chem. Eur. J.* **2017**, *23*, 4870-4875.
(36) Prezzi, D.; Varsano, D.; Ruini, A.; Marini, A.; Molinari, E. Optical properties of graphene nanoribbons: The role of many-body effects. *Phys. Rev. B* **2008**, *77*, 041404.
(37) King, B. T.; Kroulík, J.; Robertson, C. R.; Rempala, P.; Hilton, C. L.; Korinek, J. D.; Gortari, L. M. Controlling the Scholl Reaction. *J. Org. Chem.* **2007**, *72*, 2279-2288.
(38) Liu, K.-H.; Hu, G.-Q.; Wang, C.-X.; Sheng, F.-F.; Bai, J.-W.; Gu, J.-G.; Zhang, H.-H. C–H Bond Functionalization of (Hetero)aryl Bromide Enabled Synthesis of Brominated Biaryl Compounds. *Org. Lett.* **2021**, *23*, 5626-5630.
(39) Tommasini, M.; Lucotti, A.; Alfè, M.; Ciajolo, A.; Zerbi, G. Fingerprints of polycyclic aromatic hydrocarbons (PAHs) in infrared absorption spectroscopy. *Spectrochim. Acta, Part A* **2016**, *152*, 134-148.
(40) Colthup, N. B.; Daly, L. H.; Wiberley, S. E. *Introduction to infrared and Raman spectroscopy, 3rd ed.*; Academic Press: San Diego, CA, 1990.
(41) Gillen, R.; Mohr, M.; Thomsen, C.; Maultzsch, J. Vibrational properties of graphene nanoribbons by first-principles calculations. *Phys. Rev. B* **2009**, *80*, 155418.
(42) Gillen, R.; Mohr, M.; Maultzsch, J. Symmetry properties of vibrational modes in graphene nanoribbons. *Phys. Rev. B* **2010**, *81*, 205426.
(43) Matsumoto, A.; Suzuki, M.; Kuzuhara, D.; Hayashi, H.; Aratani, N.; Yamada, H. Tetrabenzoperipentacene: Stable Five-Electron Donating Ability and a Discrete Triple-Layered β-Graphite Form in the Solid State. *Angew. Chem. Int. Ed.* **2015**, *54*, 8175-8178.
(44) Ivanov, I.; Hu, Y.; Osella, S.; Beser, U.; Wang, H. I.; Beljonne, D.; Narita, A.; Müllen, K.; Turchinovich, D.; Bonn, M. Role of Edge Engineering in Photoconductivity of Graphene Nanoribbons. *J. Am. Chem. Soc.* **2017**, *139*, 7982-7988.

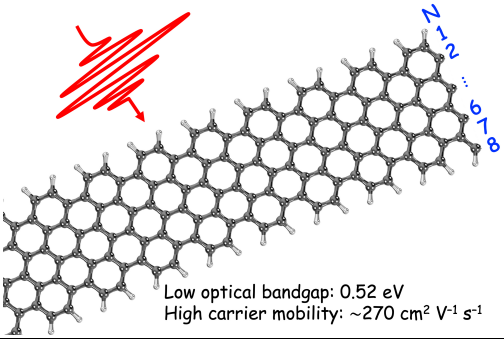
N
1
2
⋮
6
7
8
Low optical bandgap: 0.52 eV
High carrier mobility: ~270 cm² V⁻¹ s⁻¹